Neural-Network Security-Boundary Constrained Optimal Power Flow

Victor J. Gutierrez-Martinez, Claudio A. Cañizares, *Fellow, IEEE*, Claudio R. Fuerte-Esquivel, *Member, IEEE*, Alejandro Pizano-Martinez, and Xueping Gu

***Abstract*—This paper proposes a new approach to model stability and security constraints in Optimal Power Flow (OPF) problems based on a Neural Network (NN) representation of the system security boundary (SB). The novelty of this proposal is that a closed form, differentiable function derived from the system´s SB is used to represent security constraints in an OPF model. The procedure involves two main steps: First, an NN representation of the SB is obtained based on Back-Propagation Neural Network (BPNN) training. Second, a differentiable mapping function extracted from the BPNN is used to directly incorporate this function as a constraint in the OPF model. This approach ensures that the operating points resulting from the OPF solution process are within a feasible and secure region, whose limits are better represented using the proposed technique compared to typical security-constrained OPF models. The effectiveness and feasibility of the proposed approach is demonstrated through the implementation, as well as testing and comparison using the IEEE 2-area and 118-bus benchmark systems, of an optimal dispatch technique that guarantees system security in the context of competitive electricity markets.**

***Index Terms*—Neural network, optimal power flow, power system security, power system stability.**

I. Glossary of Terms

BPNN – Back-propagation Neural Network
MSV – Minimum Singular Value
NN – Neural Network
OPF – Optimal Power Flow
SB – Security Boundary
SBC-OPF – Security-boundary Constrained OPF
SC-OPF – Security-constrained OPF
SSC-OPF – Small-perturbation Stability-Constrained OPF
VSC-OPF – Voltage-stability-constrained OPF

Accepted for publication March 2010.

This work was supported by CONACyT of Mexico and the Natural Sciences and Engineering Research Council (NSERC) of Canada.

Victor J. Gutierrez-Martinez, Claudio R. Fuerte-Esquivel, and Alejandro Pizano-Martinez are with the Electrical Engineering Faculty, Universidad Michoacana de San Nicolás de Hidalgo (UMSNH), Morelia, Michoacan, 58000, Mexico (email:cfuerte@zeus.umich.mx).

Claudio A. Cañizares is with the Department of Electrical and Computer Engineering, University of Waterloo, Waterloo, ON, N2L 3G1, Canada (email:ccanizar@uwaterloo.ca).

Xueping Gu is with the School of Electrical and Electronic Engineering, North China Electric Power University, Baoding, Hebei, 071003, China (email:mexpgu@yahoo.com.cn).

II. Introduction

Power systems are currently operating close to their control and operational limits due to a variety of reasons, and as a consequence, stability problems, particularly voltage collapse and oscillatory instabilities, occur with some frequency [1]. This has led to concerns on the part of system operators regarding the secure operation of power networks, particularly in the new competitive electricity market environment [2]. In these markets, security is measured through "system congestion" levels, which have a direct effect on market transactions and electricity prices, and are represented by means of power transfer limits on main transmission corridors between operating areas. The problem with these limits is that they do not always represent the actual security limits directly associated with the current market and system conditions, given the variability of dispatch due to economic drivers, resulting in some cases in insecure operating conditions and/or inappropriate price signals [3], [4].

Better market and system operating conditions may be attained when system security is better accounted for in typical electric energy auction systems. Hence, various approaches to approximate this region in OPF models have been proposed. For example, in [5], a stability-constrained OPF model is proposed based on a time-domain numerical representation of the dynamic equations which are included as constraints in the OPF process. A somewhat similar approach is used in [6] to develop a time-domain dispatch algorithm that considers contingencies. On the other hand, in [7], the authors use the MSV of the power flow Jacobian, which is an index to detect proximity to voltage instability [8], as a security constraint to develop a VSC-OPF restricting the resulting operating points to be within certain "reasonable" distance from voltage collapse. An enhancement to this approach is presented in [9], where oscillatory and voltage instability conditions are used to develop an SSC-OPF based on the inclusion of a "dynamic" MSV stability index. In [7] and [9], the proposed stability index is an implicit function of the optimization variables, and hence their derivatives can be only approximated numerically in order to be included in the OPF solution process; this approach presents some implementation and numerical problems. An improvement to this approach is presented in [10], where an equivalent constraint based on a singular value decomposition of the

power flow Jacobian is proposed to explicitly represent the MSV constraint in the OPF model.

An alternative approach to include security constraints in an OPF model is to introduce a differentiable function representing the SB as a constraint in the model, as proposed in [11]. In this case, the stability boundary is approximated by a polynomial obtained from an interpolation procedure and a nonlinear transformation applied to the system state variables. A similar conceptual idea is proposed in this paper to include security constraints in an OPF model, but based in a differentiable function extracted from an NN which represents the stability/security boundary.

Extensive research has been carried out on the application of NNs to properly represent power system stability/security margins. For example, in [12], an approach based on an NN to assess power system stability based on training samples from off-line stability studies is presented. In [13], state-variable values are computed for a given set of contingencies, and these are then used as inputs to an NN to predict a transient stability margin. Similarly, making use of nomograms, the system SB is characterized in [14] by means of critical system parameters randomly generated to yield an NN input training set; the NN is then trained and tested to obtain an SB representation. A BPNN is used in [15] to predict voltage instabilities using as inputs both system load information and a voltage stability index; based on these inputs, the BPNN predicts new voltage stability index values for different operating scenarios. In [16], a representation of the system stability boundary based on a trained BPNN is proposed for predicting the available transfer capability of a system for any given dispatch. Finally, in [17] an NN is used to evaluate the sensitivities of a stability index based on a transient energy function method with respect to the generator power outputs for multiple contingencies, and these sensitivities are then introduced in the objective function of an OPF to indirectly account for system security in the dispatch process; this method approximately accounts for system security in the OPF process, as opposed to directly representing these security margins as constrains in the OPF model, as proposed in the present paper.

The current paper proposes a novel approach based on BPNNs to obtain explicit differentiable functions of the system stability/security boundaries. This allows the introduction of the boundaries characterized by BPNNs as constraints in OPF models. In order to achieve this goal, SBs as defined in [18] are constructed, and then the BPNNs are trained and tested to accurately represent these boundaries. From these BPNNs, explicit, differentiable functions of the OPF variables are obtained, which are then introduced as constraints in an OPF model. An SBC-OPF model for optimal dispatch in the context of competitive electricity markets is proposed, illustrated and tested using a couple of realistic IEEE test systems.

The rest of the paper is structured as follows: Section III presents and discusses some relevant SC-OPF auction models. Section IV describes the proposed SBC-OPF model; the description of the BPNN-based technique to estimate the SBs and the representation of these boundaries as explicit functions are also presented in this section. Section V discusses and compares the results obtained from the implementation and application of the SBC-OPF model to the IEEE 2-area and IEEE 118-bus benchmark systems, demonstrating the feasibility and benefits of the proposed BPNN SB and SBC-OPF. Finally, the main results and contributions of this paper are summarized and highlighted in Section VI.

III. Background Review

In this section, a brief discussion of a typical SC-OPF auction model and a recently proposed "dynamic" SC-OPF model, relevant to the technique proposed here, are presented. The advantages and disadvantages of these models are also briefly discussed.

A. SC-OPF Model

The following is a typical SC-OPF auction model, which includes the ac power flow equations as part of the optimization auction constraints to directly account for reactive power and voltage control and their associated limits [3]:

$$\begin{aligned}
\text{Min.} \quad & S_b = -\left(C_d^T P_d - C_s^T P_s\right) \\
\text{s.t.} \quad & F_{PF}\left(\delta, V, Q_g, P_s, P_d\right) = 0 \\
& 0 \le P_s \le P_{s_{\max}} \\
& 0 \le P_d \le P_{d_{\max}} \\
& P_{ij}\left(\delta, V\right) \le P_{ij_{\max}} \quad \forall i, j, i \ne j \\
& I_{ij}\left(\delta, V\right) \le I_{ij_{\max}} \quad \forall i, j, i \ne j \\
& Q_{s_{\min}} \le Q_s \le Q_{s_{\max}} \\
& V_{\min} \le V \le V_{\max}
\end{aligned} \tag{1}$$

where C_s and C_d are vectors of supply and demand bids in \$/MWh, respectively; P_s and P_d are the supply and demand power levels in MW, respectively, which cannot exceed their maximum values; $F_{PF}(\cdot)$ stands for the power flow equations of the system; V and δ correspond to the bus voltage phasor components; Q_s stands for the generator reactive powers; and I_{ij} represents the current in the transmission line ij, so that thermal limits can be directly modeled in the auction process. Finally, $P_{ij\max}$ is used to represent transmission system security limits, which are determined off-line by means of stability and contingency studies. It is important to highlight the fact that these security limits do not correspond to the actual system conditions associated with the resulting solutions, since these limits were not necessarily obtained using the operating conditions corresponding to the solution of the OPF-based auction; hence, this model may yield insecure operating conditions and/or inappropriate price signals [3], [4].

B. Dynamic SC-OPF Model

A technique to obtain a better representation of the SB, which accounts for system dynamics that can be represented

as an explicit function constraint in the OPF model, is presented in [11]. In this case, the SC-OPF model may be formulated as follows:

$$\text{Min.} \quad S_b = -\left(C_d^T P_d - C_s^T P_s\right) \tag{2}$$

$$\text{s.t.} \quad F_{PF}\left(\delta, V, Q_g, P_s, P_d\right) = 0 \tag{3}$$

$$0 \le P_s \le P_{s_{\max}} \tag{4}$$

$$0 \le P_d \le P_{d_{\max}} \tag{5}$$

$$I_{ij}\left(\delta, V\right) \le I_{ij_{\max}} \qquad \forall i, j, i \ne j \tag{6}$$

$$Q_{g_{\min}} \le Q_g \le Q_{g_{\max}} \tag{7}$$

$$V_{\min} \le V \le V_{\max} \tag{8}$$

$$f_{NRo} - f_{NR}\left(V, \delta\right) \le 0 \tag{9}$$

where the SB is represented by the explicit function $f_{NR}(\cdot)$ in (9), and f_{NRo} is a suitable threshold value. To obtain the mapping function $f_{NR}(\cdot)$, a nonlinear regression fitting technique is used. The importance of this approach is that the trained mapping function can provide a "quick" mapping between an operating point and the corresponding security status, i.e. it can be used to guarantee that the solution to the OPF problem remains within the SB defined by (9). This technique represents an advance in terms of efficiently characterizing the SB with respect to previously proposed SC-OPF methods. Hence, a similar conceptual idea is adopted in this paper to develop the proposed NN-based SBC-OPF model.

IV. Neural Network SBC-OPF

An alternative approach to include static and dynamic security constraints into the OPF formulation is discussed here. Thus, an SB is first constructed by loading the power system until the stability limits are reached for the worst single contingency (N-1 contingency criterion), for multiple and realistic generator dispatch patterns. A BPNN is then trained to approximate this boundary for each dispatch pattern, and a closed-form differentiable function that provides a mapping between the loading variables and the system's security status is generated for each considered generation pattern. These explicit functions are finally used as constraints in an OPF model somewhat similar to the model (2)-(9).

A. Definitions

A power system can be represented by a set of parameter-dependent differential equations that are constrained by a set of nonlinear algebraic equations as follows [18]:

$$\begin{aligned} \dot{x} &= h\left(x, y, \rho, \lambda\right) \\ 0 &= g\left(x, y, \rho, \lambda\right) \end{aligned} \tag{10}$$

where x is a vector of dynamic state variables corresponding to various system components, such as generators and their controls; y is a vector of "instantaneous" state (algebraic) variables, such as complex nodal load voltages; ρ is a vector of controllable parameters, such as generator terminal voltage magnitude settings; and λ is a vector of non-controllable parameters, such as load active and reactive power levels, which change continuously, moving the system from one equilibrium point to another, if the system remains stable.

The region in parameter space where all the operating points can be reached without causing instability is called a feasible region [19]. At the boundary of this region, the system equilibrium points change their stability characteristics. This feasible region and associated boundary can be constructed based on stability analyses of the differential-algebraic equations (10) representing the power system.

In the operation of power systems, the system loads and generators vary throughout the operating horizon. For a given generation dispatch pattern, each specific pattern or "direction" of load change (load increases are typically more relevant from a security standpoint than load reductions), the operating point may reach the system's feasibility boundary, driving the system to unstable conditions. Therefore, an SB can be constructed through voltage, angle and frequency stability studies for various loading changes and considering an N-1 contingency criterion. Thus, as a first step to define this boundary, let $\lambda_i = [\lambda_{i1}\ \lambda_{i2}\ \ldots\ \lambda_{iN}]^T$ be an i^{th} particular set of load increase rates for the N loads in (10), so that:

$$\begin{aligned} \lambda_{i1} &= \alpha d_{i1} \\ \lambda_{i2} &= \alpha d_{i2} \\ &\ldots \\ \lambda_{iN} &= \alpha d_{iN} \end{aligned} \tag{11}$$

where $\alpha \ge 0$ is a scalar typically referred to as the loading factor, and d_{ij}, j=1,2,…,N, represents the loading increase "direction" for load j in the i^{th} particular set of load increase rates, with the following conditions:

$$0 \le d_{ij} \le 1 \quad \forall j \tag{12}$$

$$\sum_{j=1}^{N} d_{ij} = 1 \tag{13}$$

Thus, assuming a constant power factor, the load may be defined as:

$$\begin{aligned} P_{dij} &= \lambda_{ij} P_{dj0} = \alpha d_{ij} P_{dj0} \\ Q_{dij} &= \lambda_{ij} Q_{dj0} = \alpha d_{ij} Q_{dj0} \end{aligned} \tag{14}$$

where P_{dj0} and Q_{dj0} are the "base" active and reactive powers at the j^{th} load bus.

Once the loading direction $d_i = [d_{i1}\ d_{i2}\ \ldots\ d_{iN}]^T$ is defined, the system load can be increased until an SB is reached by increasing the loading factor α; this boundary can then be associated with "critical" λ^c_{ij} values. To obtain a discrete representation of the SB, the N system loads can be varied in M different sets of load directions for given generation dispatch criteria. The SB can then be represented in the λ-parameter space, where the coordinate axes correspond to the load increase rates of the various system loads. Computationally, this boundary may be approximated by means of a critical load matrix as follows:

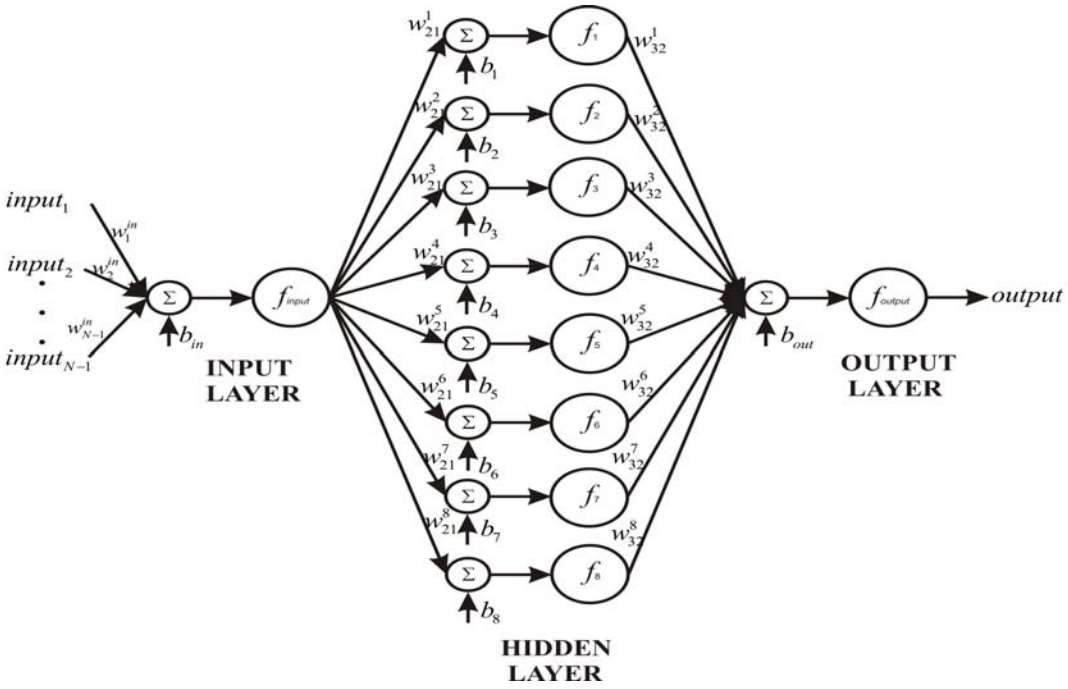

Fig. 1. BPNN architecture.

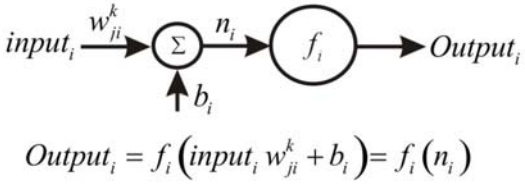

$$Output_i = f_i\left(input_i\, w_{ji}^k + b_i\right) = f_i\left(n_i\right)$$

Fig. 2. Neuron single structure.

$$M_\lambda = \begin{bmatrix} c_1 & c_2 & \cdots & c_N \end{bmatrix} = \begin{bmatrix} \lambda_{11}^c & \lambda_{12}^c & \cdots & \lambda_{1N}^c \\ \lambda_{21}^c & \lambda_{22}^c & \cdots & \lambda_{2N}^c \\ \vdots & \vdots & \ddots & \vdots \\ \lambda_{M1}^c & \lambda_{M2}^c & \cdots & \lambda_{MN}^c \end{bmatrix} \quad (15)$$

Observe that for each generation pattern considered, a similar matrix can be obtained.

The loading directions should cover the whole range $0 \le d_{ij} \le 1$ to get a complete boundary, and should have an even distribution. To get this even distribution in a multi-dimensional d-parameter space, the interval [0 1] on each axis is divided into M points, i.e. i=1, 2,…, M, where M is selected so that a reasonable density is achieved. Thus, all the possible combinations of the points that satisfy (13) can be used to obtain the boundary points required to train the BPNN.

B. SB Determination Procedure

The critical λ_{ij}^c values that define the SB for the system model (10) and a given generation dispatch are computed using continuation power flows, eigenvalue analyses and transient stability studies considering an N-1 contingency criterion, as described in some detail in [16]. These critical points obtained along different loading directions for different generation patterns, which make up the SB, constitute the training and testing sets of the BPNN.

It is important to mention that for each contingency and dispatch scenario a unique stability limit, which is a point of the stability boundary, can be obtained. The SB is then made up of the stability limit points obtained for each system dispatch and its corresponding "worst" contingency, i.e. the contingency that yields the smallest loading margin associated with the system stability limit for the given dispatch, as per the N-1 contingency criterion. Observe that if no contingencies are considered, a stability boundary rather than an SB is obtained.

C. BPNN Nonlinear Function Representation

The universal approximation theorem provides the mathematical justification for the robust approximation of any arbitrary continuous function by a nonlinear input-output mapping using BPNN [20]. Therefore, the BPNN is selected as a tool to map the SB. The mapping process for each boundary involves the following steps:

1) Obtain the matrix M_λ, which constitutes the training and testing sets for the BPNN.
2) Train and test the BPNN.
3) Obtain an explicit function representation of the BPNN for inclusion in an OPF model.

The BPNN is composed of three layers: input, hidden and output, as per Figs. 1 and 2. Each layer contains a number of neurons whose connections increase the NN's capability to learn complex relationships. The number of neurons was determined considering a compromise between the bias and the variance errors. As it is shown in Fig. 2, every connection between the i^{th} layer and the j^{th} consecutive layer through the k^{th} neuron is weighted by a number w_{ji}^k. A neuron adds the incoming inputs $input_i$, which could be the weighted output information from other neurons, and passes the net sum

through an activation function f_i. The activation function of each neuron transforms the net weighted sum n_i of all incoming input signals into one output signal. Also, each neuron has an additional input, called a bias b_i, which is used in the network to generalize the solution and avoid a zero value for n_i, even when an $input_i$ is zero.

The BPNN architecture used in this paper was selected based on the criteria of having the simplest neurons array, capable to map the security or stability boundary with a reasonable degree of precision. Hence, it consists of one neuron for both input and output layers, and eight neurons for the hidden layer, as shown in Fig. 1. The neurons making up the hidden layer have the activation function:

$$f_i\left(n_i\right)=\left(\frac{2}{1+e^{-2n_i}}\right)-1 \tag{16}$$

where n_i can be an input state variable or algebraic expression, depending on the state variables coming from the input data or output from other neurons. The input and output neurons have a linear activation function with unitary value.

The input-output relationship of the neuron single structure is shown in Fig. 2. From the input-output relationships between the three layers of the trained BPNN shown in Fig. 1, it is possible to obtain the implicit mapping function that explicitly relates the BPNN inputs and output. Thus, for the input layer, the input-output relationship can be written as:

$$Output_{in}=input_i w_i^{in}+b_{in}\ \ \forall i=1,...,N-1 \tag{17}$$

This constitutes the input of the hidden layer; therefore, the input-output relationship at each neuron of this layer is:

$$Output_k=f_k\left(\left(input_i w_i^{in}+b_{in}\right)_k w_{21}^k+b_k\right)w_{32}^k\ \ \forall k=1,...,8 \tag{18}$$

Since these outputs form the input of the output layer, the following mapping function can be obtained:

$$\begin{aligned}Output_{out}=&\sum_{k=1}^{8} f_k\left(\left(input_i w_i^{in}+b_{in}\right)_k w_{21}^k+b_k\right)w_{32}^k\\&+b_{out}\quad \forall i=i,...,N-1\end{aligned} \tag{19}$$

Once the BPNN has been trained and tested, and thus its weighted values have been computed, one can use (19) as the closed form, differentiable function that represents the boundary, as explained in Section IV.E.

D. BPNN Training and Testing

The method used to train the BPNN off-line consists on iteratively adjusting the network weights and biases to minimize a network performance function, which in this work is given by the mean square error between the network outputs and the target outputs. The gradient of the performance function is used to determine how to adjust all the weights and biases, using an updating technique known as back-propagation; this technique starts at the output layer and propagates the results backwards to the input layer. The Levenberg-Marquardt algorithm is used in the present work to minimize the performance function based on its gradient, since it has an adequate performance and it is not affected by the accuracy required on the function approximation [21].

In order to train the NN, the M critical values of each $N-1$ loading points making up the boundary are provided as inputs to the NN, i.e. in Fig. 1, $input_1 = c_1$, $input_2 = c_2$,..., $input_{\ell-1} = c_{\ell-1}$, $input_\ell = c_{\ell+1}$,…, and $input_{N-1} = c_N$, as per (15). The target (output) value that must be satisfied within a given tolerance is given by a chosen ℓ^{th} column of M_λ, i.e. $Output_{out} = c_\ell$, so that $c_\ell = f(input)$, where $input = [input_1 \ \ldots \ input_{N-1}]$, and $f(\cdot)$ stands for the "total" NN function (19). Observe that a given point on the boundary is basically defined by:

$$\begin{aligned}\lambda_{i\ell}^c &\approx f\left(\lambda_{i1},\lambda_{i2},\cdots,\lambda_{i\,\ell-1},\lambda_{i\,\ell+1},\cdots,\lambda_{iN}\right)\\&\approx f\left(\hat{\lambda}_i\right)\end{aligned} \tag{20}$$

In other words, for N-1 known load increase rates defined by the vector $\hat{\lambda}_i$, the SB value $\lambda_{i\ell}^c$ of a chosen ℓ^{th} load increase is basically defined by (20).

The boundary points can also be represented in the P_d-parameter or loading space based on (11), (14) and (20), so that a critical loading point on the boundary is given by:

$$\begin{aligned}P_{di\ell}^c &\approx f\left(P_{di1},P_{di2},\cdots,P_{di\,\ell-1},P_{di\,\ell+1},\cdots,P_{diN}\right)\\&\approx f\left(\hat{P}_{di}\right)\end{aligned} \tag{21}$$

Therefore, the equation:

$$P_{d_\ell}^c-f\left(\hat{P}_d\right)=0 \tag{22}$$

defines a hypersurface in the N-dimensional loading space on which the BPNN SB is defined (e.g. for 2 loads it is a curve, for 3 loads it is a 2-dimensional surface, etc.).

The BPNN training and validation process used here is based on randomly dividing the input vectors and the target vector in three sets as follows: 60% are used for training; 20% are used to validate the NN network and to stop training before over-fitting as per the abovementioned performance function; and the last 20% are used as an independent set to test the BPNN generalization [21]. The time that it takes to train the BPNN is in the range of a few seconds to several minutes, depending of the number of loads or loading areas considered to build the SB. Hence, since this is carried out off-line, obtaining the required BPNN SBs should not represent a problem in a practical implementation of the proposed methodology.

E. BPNN Mapping Nonlinear Function

It is shown in [22] that the linearized power flow mismatch equations can be represented using an NN. In this case, the interconnections of layers represent the Jacobian matrix elements, while the weighted numbers w_{ji}^k are related to the values of these elements. Bearing this in mind, and following an inverse procedure, it is possible to use a symbolic algebraic process to relate the NN output and input to the BPNN, considering its architecture and the basic neuron structure, as shown in the previous section. Hence, the mapping function that relates the input-output for the BPNN shown in Fig. 1, in terms of load increase rates, is obtained from (19) and (20) as:

$$\lambda_\ell^c = \sum_{k=1}^{8} f_k\left(\left(\hat{\lambda}^T w^{in} + b_{in}\right) w_{21}^k + b_k\right) w_{32}^k + b_{out} \quad (23)$$

where $w^{in}=[w_1^{in}\ w_2^{in}\ \ldots\ w_{N-1}^{in}]^T$. From (11), (23) can be rewritten as:

$$\alpha^c d_\ell = \sum_{k=1}^{8} f_k\left(\left(\hat{\lambda}^T w^{in} + b_{in}\right) w_{21}^k + b_k\right) w_{32}^k + b_{out} \quad (24)$$

where α^c represents the critical loading factor. Observe that the system operating point associated with a loading level $\lambda_\ell > \lambda_\ell^c$ is located outside the security region.

Based on (14), it is possible to express the mapping function (23) as:

$$P_{d\ell}^c = \sum_{k=1}^{8} f_k\left(\left(\hat{P}_d^T w^{in} + b_{in}\right) w_{21}^k + b_k\right) w_{32}^k + b_{out} \quad (25)$$

Similarly, system operating points associated with a loading level $P_{d\ell} > P_{d\ell}^c$ are located outside the security region. Hence, the mapping functions (23) or (25) can be used as security constraints in the OPF formulation, as explained next.

F. Security Boundary Constrained OPF Model

Given that in practice the majority of system loads are inelastic [23], i.e. price unresponsive, the OPF model (2)-(9) that is the basis for the OPF dispatch model presented here can be readily modified to reflect this fact. Thus, the proposed optimization model considers that loads bid on the market only a fraction of their demand which they are willing to curtail if need be at a high curtailment price; this reflects better the way markets operate in most jurisdictions. Furthermore, the security constraint (9) is replaced by the proposed BPNN SB (23) for each supply pattern considered. Therefore, the following OPF model is proposed:

$$\text{Min.} \quad S_b = C_s^T P_s - C_d^T \Delta P_d \quad (26)$$

$$\text{s.t.} \quad F_{PF}\left(\delta, V, Q_g, P_s, P_d, Q_d\right) = 0 \quad (27)$$

$$0 \le P_s \le P_{s\max} \quad (28)$$

$$Q_{s\min} \le Q_s \le Q_{s\max} \quad (29)$$

$$V_{\min} \le V \le V_{\max} \quad (30)$$

$$\lambda_\ell - \sum_{k=1}^{8} f_{k_m}\left(\left(\hat{\lambda}^T w_m^{in} + b_{in_m}\right) w_{21_m}^k + b_{k_m}\right) w_{32_m}^k + b_{out_m} \le 0 \qquad \forall m = 1,\ldots,G \quad (31)$$

$$\Delta P_{dj} \le 0 \quad \forall j = 1,\ldots,N \quad (32)$$

$$\Delta P_{dj} = \left(\lambda_j - \lambda_{j0}\right) P_{dj0} = \left(\alpha d_j - \alpha_0 d_{j0}\right) P_{dj0} \quad \forall j = 1,\ldots,N \quad (33)$$

$$Q_{dj} = \tan\left(\varphi_j\right) P_{dj} \quad \forall j = 1,\ldots,N \quad (34)$$

$$0 \le d_j \le 1 \quad \forall j = 1,\ldots,N \quad (35)$$

$$\sum_{j=1}^{N} d_j = 1 \quad (36)$$

$$\alpha \ge 0 \quad (37)$$

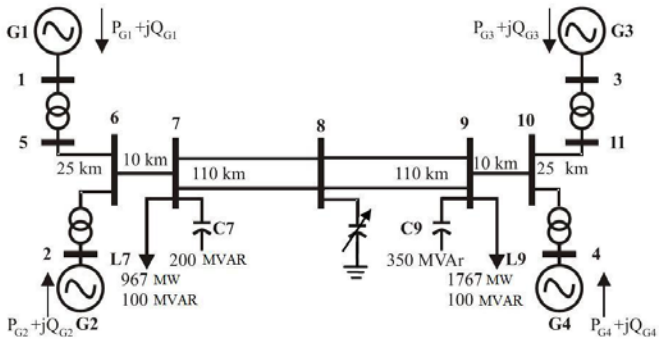

Fig. 3. IEEE 2-area benchmark system.

where m stands for the m^{th} SB obtained for a given generation pattern out of a total of G dispatch patterns; C_d represents load curtailment prices; and the load curtailments are represented by ΔP_d, assuming a constant power factor as per (35). Observe that constraints (32) force ΔP_{dj} to be negative or zero for all bidding loads, which, combined with high C_d values, would effectively force load curtailment to be zero if there is a solution to the problem within the boundaries defined by (31), becoming nonzero only when there are security violations that cannot be resolved simply with generation dispatch. It is important to highlight the fact that for loads that do not wish to bid in the market, $C_{dj} = \Delta P_{dj} = 0$. Therefore, this optimization dispatch model properly reflects the basic operating principles for electricity markets dispatch nowadays.

This model was solved using two different types of solvers: the Newton-based approach described in [24] and [25], and AMPL [26] with the KNITRO solver [27]. Both generated the same solutions in all the examples discussed next.

V. RESULTS

Numerical results of the proposed method are presented and discussed in this section. Comparisons between the proposed BPNN SB mapping approach and the one proposed in [11] are also presented.

Two sample systems were selected to test and demonstrate the proposed SBC-OPF model, namely, the IEEE 2-area system and the IEEE 118-bus system; the latter allows demonstrating that the presented approach can be readily applied to realistic power systems. To simplify the presented analyses and explanations of the results, and without loss of generality, the SB was obtained for a "typical" dispatch pattern, i.e. G =1 in (31) for both test systems. Furthermore, to test the effect of the security constraint (31), all case studies presented are based on load dispatches P_{do} that violate the SBs.

A. IEEE 2-area Benchmark System

The slightly modified IEEE 2-area benchmark shown in Fig. 3 consists of two similar areas connected through a relatively weak double-circuit tie line; the added variable capacitor at Bus 8 keeps the bus voltage constant to improve voltage profiles for various loading conditions. The system generators were modeled using detailed subtransient models including

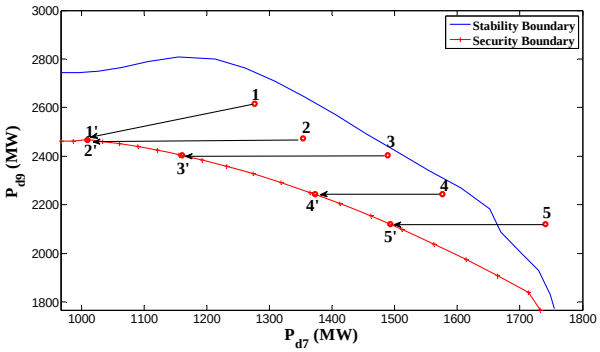

Fig. 4. Security and stability boundaries for the IEEE 2-area system.

simple excitation systems and speed governors. A power system stabilizer was installed on generator G4 to damp possible low frequency oscillations. There are only two loads in the system at Buses 7 and 9, respectively. The system data can be found in [30], and Table I depicts the generator bid data and limits used in the simulations.

Following the procedure described in Section IV-B, the SB was obtained based on 21 different loading directions for each load, and detailed static and dynamic studies using the tools described in [28] and [29]; the generator dispatch pattern used to obtain the boundary was based on the base generator powers. To train the NN, λ_{i7}^{c} was assumed as the input to the BPNN, and λ_{i9}^{c} was considered as the target; it took about 91 s on a standard PC to minimize the error between the output and the target to within a 10^{-5} tolerance. The resulting stability and SBs are depicted in Fig. 4. The latter corresponds to the system stability boundary for a Line 7-8 trip, which is not the worst contingency in this test system, since other line trips such as a Line 6-7 trip would yield an unsolvable base power flow; however, this suffices to illustrate the application of the proposed dispatch algorithm without loss of generality. Observe the reduced loadability margin when the contingency is considered. Note as well that the boundaries present some discontinuities that are "averaged" by the NN approximation, which is a differentiable nonlinear function in the considered loading space.

The values for α, d_{i7} and d_{i9} shown in Table II were chosen, so that the corresponding P_{d7} and P_{d9} values force the system to be outside the SB to test the proposed optimization model, which should yield the most economical dispatch while meeting all security constraints. The base load values are depicted in Fig. 3. The assumed large curtailment bids for the loads were C_{d7} = 200 \$/MWh and C_{d9} = 2200 \$/MWh, which are, as previously discussed, significantly larger than the generator bids, which are in the 70 to 90 \$/MWh range.

The load change results obtained by applying the proposed model (26)-(37) are shown in Table III, and Table IV shows the corresponding generator dispatches. The 5 initial loading points and 5 final points with respect to the SB are shown in Fig. 4; observe how the loads are minimally curtailed so that the system returns to its SB, curtailing the cheapest load the most, as expected. Thus, in all cases, the cheapest load P_{d7} is curtailed the most, whereas the most expensive load P_{d9} is only curtailed in the cases when this is necessary to bring the system within the security limits (Cases 1 and 2), which is clearly illustrated with Fig. 4.

The proposed BPNN SB representation (23) was then replaced by the following polynomial approximation proposed in [11]:

$$\lambda_{\ell}^{c} = A + \sum_{\substack{i=1 \\ i\neq \ell}}^{N} \left(B_i \hat{\lambda}_i + \sum_{\substack{j=i+1 \\ i\neq \ell}}^{N} C_{ij} \hat{\lambda}_i \hat{\lambda}_j + D_i \hat{\lambda}_i^{2} \right) \qquad (38)$$

TABLE I
POWER GENERATION BIDS FOR THE 2-AREA SYSTEM

Gen.	C_s [\$/MWh]	$P_{s\max}$ [MW]
G1	70	900
G2	70	1000
G3	90	900
G4	70	900

TABLE II
IEEE 2-AREA SYSTEM LOADING SCENARIOS

Case	α	d_{i7}	d_{i9}	P_{d_7} [MW]	P_{d_9} [MW]
1	0.8	0.4	0.6	1276.44	2615.16
2	0.8	0.5	0.5	1353.80	2473.80
3	0.9	0.6	0.4	1489.18	2403.12
4	0.9	0.7	0.3	1576.21	2244.09
5	1.0	0.8	0.2	1740.60	2120.40

TABLE III
IEEE 2-AREA SYSTEM LOAD CURTAILMENT VALUES

Case	α	d_{i7}	d_{i9}	ΔP_{d_7} [MW]	ΔP_{d_9} [MW]
1	0.4402	0.1004	0.8996	266.68	148.38
2	0.4402	0.1004	0.8996	344.04	7.02
3	0.5602	0.3574	0.6426	328.56	0.0
4	0.6902	0.6088	0.3912	202.90	0.0
5	0.7436	0.7310	0.2690	247.93	0.0

TABLE IV
IEEE 2-AREA SYSTEM GENERATOR OUTPUTS

Case	P_{G1} [MW]	P_{G2} [MW]	P_{G3} [MW]	P_{G4} [MW]
1	900	1000	689	900
2	900	1000	689	900
3	900	1000	776	900
4	900	1000	829	900
5	900	1000	825	900

TABLE V
IEEE 2-AREA SYSTEM LOAD CURTAILMENT VALUES

	NN APPROACH			NR APPROACH		
Case	ΔP_{d_7} [MW]	ΔP_{d_9} [MW]	(31)	ΔP_{d_7} [MW]	ΔP_{d_9} [MW]	(38)
1	266.68	148.38	-2.2e-5	309.44	148.60	2.3e-5
2	344.04	7.02	-2.2e-5	386.80	7.24	2.3e-5
3	328.56	0.0	-1.8e-5	321.66	0.0	2.2e-5
4	202.90	0.0	1.4e-5	207.12	0.0	-7.4e-5
5	247.93	0.0	3.1e-6	246.75	0.0	-2.6e-5

TABLE VI
POWER GENERATION BIDS FOR THE 118-BUS SYSTEM

Gen.	C_s [$/MWh]	Gen.	C_s [$/MWh]	Gen.	C_s [$/MWh]
1	30	19	30	37	30
2	30	20	30	38	30
3	30	21	50	39	80
4	80	22	30	40	30
5	30	23	30	41	30
6	50	24	30	42	30
7	30	25	40	43	30
8	30	26	40	44	40
9	30	27	30	45	30
10	30	28	40	46	30
11	60	29	70	47	30
12	70	30	30	48	30
13	30	31	30	49	30
14	30	32	30	50	30
15	30	33	30	51	30
16	30	34	30	52	30
17	30	35	30	53	30
18	30	36	90	54	30

TABLE VII
118-BUS SYSTEM 3-AREA LOADING SCENARIOS

Case	$P_{d_{A1}}$ [MW]	$P_{d_{A2}}$ [MW]	$P_{d_{A3}}$ [MW]
1	848.64	822.97	2138.85
2	866.944	803.794	2061.444
3	836.16	830.96	2047.185

A nonlinear regression (NR) approach was used to obtain the *A*, *B*, *C* and *D* parameters in (38). A similar procedure used for the validation of the NN is used for validating the NR; thus, 70% of input and target vectors are used in the fitting process, while the rest are used to validate the NR function performance. The resulting mean square errors for the NN and the NR functions are 9.94e-7 and 2.39e-5, respectively, which basically shows that the NN approximation fits the boundary better than the NR polynomial approximation. Table V shows the load changes and the value of the corresponding SB constraint for the NN approximation (31) and the NR approximation (38). Observe that the differences in load curtailments are not significant, but the NN security constraint is in general closer to zero than the NR polynomial one, thus yielding more accurate results, at similar computational costs for the solution of the optimization model. Considering that both approximations are based on the same training data, with the NN approach requiring a not too costly off-line training process, while the NR approach requires a computationally somewhat cheaper off-line fitting process, the NN approximation can be considered a better alternative given the more accurate results.

B. IEEE 118-bus Benchmark System

To prove the effectiveness of the proposed method with a more realistic system, the IEEE 118-bus benchmark system was used to test it. The system is composed of 53 generators and 91 loads. The data are available in [31], and the generator bid data are given in the Table VI.

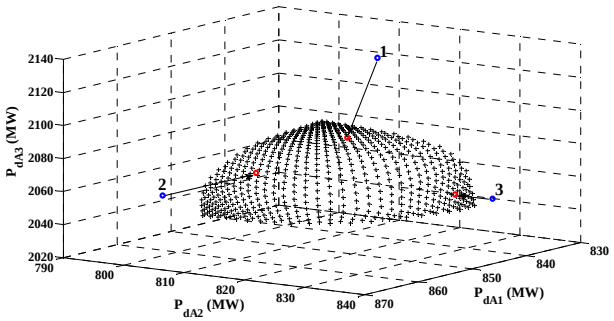

Fig. 5. SB for the IEEE 118-bus system for three areas.

TABLE VIII
118-BUS SYSTEM 3-AREA LOAD CURTAILMENT VALUES

Case	$\Delta P_{d_{A1}}$ [MW]	$\Delta P_{d_{A2}}$ [MW]	$\Delta P_{d_{A3}}$ [MW]
1	10.1147	13.9695	62.4044
2	17.3010	0.0	0.0
3	0.0	6.2105	0.0

Following standard utility and electricity market practices, the system was divided in both 3 and 4 operational areas, so that the corresponding SBs basically represent transfer limits between these areas. The proposed BPNN SBs were obtained in both cases using, for the sake of simplicity and without loss of generality, voltage stability criteria only, i.e. the boundary is basically composed of saddle-node and limit-induced bifurcations [29], [32], and assuming that a Line 39-40 trip stands for the worst contingency. A total of 631 loading directions were considered to get an even distribution of training points, and a generation dispatch pattern based on the base generator powers was used. A similar training and testing procedure to the one used for the IEEE 2-area system was applied to obtain the required security boundaries.

1) *Three Areas:* The system was divided in three operating areas, namely, Area 1 with 31 loads; Area 2 with 31 loads; and Area 3 with 29 loads. The SB mapped by the proposed BPNN is illustrated in Fig. 5 in the P_d-parameter space; it took 156 s on a standard PC to train the BPNN. The three area loading cases shown in Table VII, which all define operating conditions outside the security region as depicted in Fig. 5, were used to test the proposed optimal dispatch model, with the following large load curtailment bids per area: C_{dA1} = 200 $/MWh, C_{dA2} = 400 $/MWh, and C_{dA3} = 600 $/MWh. The total area loads were proportionally distributed among the area buses based on their base loading values.

Table VIII shows the total area load changes resulting from the solution of the dispatch model (26)-(37), which also yields optimal dispatch values for all generators. Observe in Fig. 5 how the most expensive Area 3 loads are shed the least, except for Case 1, where this load must also be curtailed for the system to be on the required SB.

As in the case of the IEEE 2-area system, a comparison between the NN and NR approaches to map the SB was also

TABLE IX
118-BUS SYSTEM 4-AREA LOADING SCENARIOS

Case	$P_{d_{A1}}$ [MW]	$P_{d_{A2}}$ [MW]	$P_{d_{A3}}$ [MW]	$P_{d_{A4}}$ [MW]
1	790.0891	623.6631	1237.4465	1624.8792
2	807.7263	648.9401	1332.6901	1661.1514
3	798.8817	758.0656	1442.9201	1642.9618

TABLE X
118-BUS SYSTEM 4-AREA LOAD CURTAILMENT VALUES

Case	$\Delta P_{d_{A1}}$ [MW]	$\Delta P_{d_{A2}}$ [MW]	$\Delta P_{d_{A3}}$ [MW]	ΔP_{d4} [MW]
1	0.0	0.0	0.0001	154.0212
2	0.0	0.0	0.0	190.2934
3	0.0	0.0	0.0	172.1038

carried out. The mean square errors for the NN and the NR approximations are 2.6e-6 and 5.85e-6 respectively, showing that the NN approximates better the boundary than the NR polynomial.

2) *Four Areas:* In this case, the system was divided in the following four areas: Area 1, 2 and 3 with 22 loads each; and Area 4 with 25 loads. The BPNN SB training took 225 s in this case. The three test cases shown in Table IX were used to test the proposed dispatch model; all operating points are located outside the security region. The total area load was assumed again to be proportionally distributed among the area buses based on their base loading values. The large curtailment bids assumed for the loads in each area were: C_{dA1} = 800 \$/MWh, C_{dA2} = 100 \$/MWh, C_{dA3} = 300 \$/MWh, and C_{dA4} = 600 \$/MWh.

The load changes obtained from solving the SBC-OPF model (26)-(37) for all 3 operating cases considered are shown in Table X. The loads are curtailed according to their bids and effect on system security; in this case, the most expensive loads in Area 1 as well as the cheaper loads in Areas 2 and 3 are not curtailed, with only the loads in Area 4, which have the most impact on system security conditions, being shed the most.

VI. CONCLUSIONS

This paper proposed a new technique to obtain a differentiable function of power system variables from an NN approximation of the stability/security boundary. This function was introduced as a security constraint in an SC-OPF model for optimal dispatch in a competitive market environment, accounting for the load inelasticity in current auction and dispatch problems. It was shown that the solution of the proposed SBC-OPF problem yields dispatch conditions that are within a feasible operating region from the stability/security viewpoint. The proposed model was tested using two IEEE benchmark systems, demonstrating its usefulness and feasibility in practical applications.

The proposed approach represents a new and useful technique to deal with the issue of properly representing system congestion in OPF-based auction and dispatch mechanisms. Using the proposed SB representation, system operators should have a full and more accurate representation of the shape and characteristics of the secure operating region, allowing them to properly dispatch generator and loads, as well as take preventive and corrective actions to avoid system instabilities.

The proposed SB representation can be applied to any other OPF-based dispatch and market auction models, such as the classical dc-OPF. Given that in practice most energy dispatch and market clearing mechanisms are based on the latter, the authors are currently working on developing practical dc-OPF dispatch models based on the proposed NN SB.

REFERENCES

[1] P. Hines, J. Apt, and S. Talukdar, "Trends in the History of Large Blackouts in the United States," in *Proc. IEEE-PES General Meeting*, 8 pp., July 2008.

[2] "Final Report on the August 14, 2003 Blackout in the United States and Canada: Causes and Recommendations," *U. S. – Canada Power System Outage Task Force*, April 2004.

[3] C. A. Cañizares and S. K. M. Kodsi, "Power System Security in Market Clearing and Dispatch Mechanisms," in *Proc. IEEE-PES General Meeting*, 6 pp., June 2006.

[4] H. Ghasemi and A. Maria, "Benefits of Employing an On-line Security Limit Derivation Tool in Electricity Markets," in *Proc. IEEE-PES General Meeting*, 6pp., July 2008.

[5] D. Gan, R. J. Thomas, and R. D. Zimmerman, "Stability-Constrained Optimal Power Flow," *IEEE Trans. on Power Systems*, Vol. 15, No. 2, pp. 535-540, May 2000.

[6] S. Bruno, E. D. Tuglie, and M. La Scala, "Transient Security Dispatch for the Concurrent Optimization of Plural Postulated Contingencies," *IEEE Trans. on Power Systems*, Vol. 17, No. 3, pp. 707-714, August 2002.

[7] C. A. Cañizares, W. Rosehart, A. Berizzi, and C. Bovo, "Comparison of Voltage Security Constrained Optimal Power Flow Techniques," in *Proc. IEEE-PES Summer Meeting*, Vancouver, BC, Canada, pp. 1680-1685, July 2001.

[8] P. A. Lof, T. Smed, G. Andersson, and D. J. Hill, "Fast Calculation of a Voltage Stability Index," *IEEE Trans. on Power Systems*, Vol. 7, No. 1, pp. 54-64, February 1992.

[9] S. K. M. Kodsi and C. A. Cañizares, "Application of a Stability Constrained Optimal Power Flow to Tuning of Oscillation Controls in Competitive Electricity Markets," *IEEE Trans. on Power Systems*, Vol. 22, No. 4, pp. 1944-1954, November 2007.

[10] R. J. Avalos, C. A. Cañizares, and M. F. Anjos, "A Practical Voltage-Stability-Constrained Optimal Power Flow," in *Proc. IEEE-PES General Meeting*, July 2008.

[11] B. Jayasekara and U. Annakkage, "Derivation of an Accurate Polynomial Representation of the Transient Stability Boundary," *IEEE Transactions on Power Systems*, Vol. 21, No. 4, pp. 1856-1863, November 2006.

[12] M. Aggoune, M. A. El-Sharkawi, D. C. Park, M. J. Damborg, and R. J. Marks II, "Preliminary Results on Using Artificial Neural Networks for Security Assessment," *IEEE Trans. on Power Systems*, Vol. 6, No. 2, pp. 252-258, May 1991.

[13] A. R. Eduards, K. W. Chan, R. W. Dunn, and A. R. Daniels, "Transient Stability Screening Using Artificial Neural Networks Within a Dynamic Security Assessment," *IEE Proc. on Generation, Transmission and Distribution*, Vol. 143, No. 2, pp. 129-134, March 1996.

[14] J. D. McCalley, S. Wang, R. T. Treinen, and A. D. Papalexopoulos, "Security Boundary Visualization for Power Systems Operation," *IEEE Trans. on Power Systems*, Vol. 12, No. 2, pp. 940-947, May 1997.

[15] S. Sahari, A. F. Abdin, and T. K. Rahaman, "Development of Artificial Neural Network for Voltage Stability Monitoring," in *Proc. National Power Engineering Conference*, pp. 37-42, December 2003.
[16] X. Gu, and C. A. Cañizares, "Fast Prediction of Loadability Margins Using Neural Networks to Approximate Security Boundaries of Power Systems," *IET Generation, Transmission and Distribution*, Vol. 1, No. 3, pp. 466-475, May 2007.
[17] V. Miranda, J. N. Fidalgo, J. A. Pecas Lopes, and L. B. Almeida, "Real Time Preventive Actions for Transient Stability Enhancement with a Hybrid Neural Network – Optimization Approach," *IEEE Trans. on Power Systems*, Vol. 10, No. 2, pp. 1029-1035, May 1995.
[18] P. W. Sauer and M. A. Pai, *Power System Dynamics and Stability*. Prentice Hall, 1988.
[19] V. Venkatasubramanian, H. Schättler, and J. Zaborsky, "Local Bifurcations and Feasibility Regions in Differential-Algebraic Systems," *IEEE Transactions on Automatic Control*, Vol. 40, No. 12, pp. 1992-2013, December 1995.
[20] S. Haykin, *Neural Networks: A comprehensive foundation*. Prentice Hall, Second Edition, 1999.
[21] H. Demoth, M. Beale, and M. Hagan, "Neural Network Toolbox 6," The Mathworks Inc.
[22] T. T. Nguyen, "Neural Network Load Flow," *IEE Proc Generation, Transmission and Distribution*, Vol. 142, No. 1, pp. 51-58, January 1995.
[23] E. Bompard, E. Carpaneto, G. Chicco, and G. Gross, "The Role of Load Demand Elasticity in Congestion Management and Pricing," in *Proc. IEEE-PES SM*, July 2000, pp. 2229-2234.
[24] A. Pizano-Martinez, C. R. Fuerte-Esquivel, H. Ambriz-Perez, and E. Acha, "Modeling of VSC-based HVDC Systems for a Newton-Raphson OPF Algorithm," *IEEE Trans. Power Systems*, Vol. 22, No. 4, pp. 1794-1803, November 2007.
[25] C. R. Fuerte-Esquivel, E. Acha, S. G. Tan, and J. J. Rico, "Efficient Object Oriented Power Systems Software for the Analysis of Large Scale Networks Containing FACTS-Controlled Branches," *IEEE Trans. Power Systems*, Vol. 12, No. 2, pp. 464-472, May 1998.
[26] R. Fourer, D. M. Gay, and B. W. Kernighan, *AMPL: A Modeling Language for Mathematical Programming*, 2nd ed. Thomson, 2003
[27] KNITRO. [Online]. Available: http://www.ziena.com
[28] F. Milano, "An Open Source Power System Analysis Toolbox," *IEEE Trans. on Power Systems*, Vol. 20, No. 3, p. 1199-1206, August 2005.
[29] UWPFLOW, April 2006. [Online]. Available: http://thunderbox.uwaterloo.ca/~claudio/software/pflow.htm
[30] P. Kundur, *Power System Stability and Control*. McGraw-Hill, 1994.
[31] Power Systems Test Case Archive, Electrical Engineering, University of Washington. [Online]. Available: http://www.ee.washington.edu/research/pstca/
[32] "Voltage stability assessment: Concepts, practices and tools," IEEE/PES Power System Stability Subcommittee, Tech. Rep. SP101PSS, August 2002.

Victor J. Gutierrez-Martinez received the B.Eng. (Hons.) and the MS degrees from the Universidad Michoacana de San Nicolás de Hidalgo (UMSNH), Morelia, México, in 2000 and 2004, respectively. He is currently pursuing the PhD degree in the area of dynamic and steady-state analysis of power systems at UMSNH. From June 2007 to May 2008, he was a visiting student at the University of Waterloo.

Claudio A. Cañizares (S'85, M'91, SM'00, F'07) received in April 1984 the Electrical Engineer Diploma from the Escuela Politécnica Nacional (EPN), Quito-Ecuador, where he held different teaching and administrative positions from 1983 to 1993. His MS (1988) and PhD (1991) degrees in Electrical Engineering are from the University of Wisconsin-Madison. Dr. Cañizares has held various academic and administrative positions at the E&CE Department of the University of Waterloo since 1993, where he is currently a Full Professor and the Associate Director of the Waterloo Institute for Sustainable Energy (WISE). His research activities concentrate on the study of modeling, simulation, control, stability, computational and dispatch issues in power systems in the context of competitive electricity markets.

Claudio R. Fuerte-Esquivel (M'91) received the B.Eng. (Hons.) degree from the Instituto Tecnológico de Morelia, Morelia, México, in 1990, the MS degree (*summa cum laude*) from the Instituto Politécnico Nacional, México, in 1993, and the PhD degree from the University of Glasgow, Glasgow, Scotland, U.K., in 1997. Currently, he is an Associate Professor at the Universidad Michoacana de San Nicolás de Hidalgo (UMSNH), Morelia, where his research interests lie in the dynamic and steady-state analysis of FACTS.

Alejandro Pizano-Martinez received the B.Eng. (Hons.) degree in 1999 from the University of Colima, Colima, México, and the MS degree in 2004 from the Universidad Michoacana de San Nicolás de Hidalgo (UMSNH), Morelia, México, in 2004. He is currently pursuing the PhD degree in UMSNH in the area of dynamic and steady-state analysis of FACTS.

Xueping Gu received his MSc degree in 1988 from the Harbin Institute of Technology (China), and his PhD degree in 1996 from the North China Electric Power University (NCEPU), both in Electrical Engineering. He worked in the City University of Hong Kong as a Research Associate from July 1996 to June 1998, and as a Senior Research Associate from June 2000 to May 2001. From July 2005 to June 2006, he was a Visiting Professor at the University of Waterloo. He is currently Professor at the School of Electrical and Electronics Engineering in NCEPU. His areas of interest include application of intelligent technologies to power systems, power system security and stability, and power system restoration.